Physics of the Dark Universe 42 (2023) 101276

Contents lists available at ScienceDirect

Physics of the Dark Universe

journal homepage: www.elsevier.com/locate/dark

Cosmological constraints on dark energy in $f(Q)$ gravity: A parametrized perspective

A. Mussatayeva [a], N. Myrzakulov [b,c], M. Koussour [d,*]

[a] Department of Physics and Chemistry, S. Seifullin Kazakh Agrotechnical University, Astana 010011, Kazakhstan
[b] L.N. Gumilyov Eurasian National University, Astana 010008, Kazakhstan
[c] Ratbay Myrzakulov Eurasian International Centre for Theoretical Physics, Astana 010009, Kazakhstan
[d] Quantum Physics and Magnetism Team, LPMC, Faculty of Science Ben M'sik, Casablanca Hassan II University, Morocco

ARTICLE INFO

Article history:
Received 3 April 2023
Received in revised form 6 June 2023
Accepted 22 June 2023

Keywords:
$f(Q)$ gravity
Dark energy
EoS parameter
Cosmological constraints

ABSTRACT

In this paper, we focus on the parametrization of the effective equation of state (EoS) parameter within the framework of $f(Q)$ symmetric teleparallel gravity. Here, the gravitational action is represented by an arbitrary function of the non-metricity scalar Q. By utilizing a specific parametrization of the effective EoS parameter and a power-law model of $f(Q)$ theory, namely $f(Q) = \beta Q^{(m+1)}$ (where β and m are arbitrary constants), we derive the cosmological solution of the Hubble parameter $H(z)$. To constrain model parameters, we employ recent observational data, including the Observational Hubble parameter Data (*OHD*), Baryon Acoustic Oscillations data (*BAO*), and Type Ia supernovae data (*SNe* Ia). The current constrained value of the deceleration parameter is found to be $q_0 = -0.50^{+0.01}_{-0.01}$, indicating that the current Universe is accelerating. Furthermore, we examine the evolution of the density, EoS, and $Om(z)$ diagnostic parameters to deduce the accelerating nature of the Universe. Finally, we perform a stability analysis with linear perturbations to confirm the model's stability.

1. Introduction

In modern cosmology, the observational aspect is critical. The introduction of new tools in observation causes cosmologists to reassess the formulation of gravitational theories regularly. With the discovery of Hubble, Einstein was forced to remove the cosmological constant from his field equations in General Relativity Theory (GRT). The observation of Type Ia supernovae (*SNe* Ia) in 1998 forced cosmologists to abandon the hypothesis of decelerating Universe expansion [1,2]. Since then, the Baryon Acoustic Oscillations (*BAO*) [3,4], Cosmic Microwave Background (*CMB*) [5,6], and Large Scale Structure (*LSS*) [7,8], and many more measurements have provided evidence for the Universe's accelerated expansion. Thus, it is critical to include observable data while developing a theoretical cosmological model of the Universe. The accelerated expansion of the Universe is a key characteristic of modern cosmology. The Einstein field equations in GRT invariably result in a decelerating expansion of the Universe with the normal matter constituent. The accelerating expansion can be characterized by introducing a new constituent to the energy–momentum tensor part of the field equations or by making some changes to the geometrical part. Using these concepts, recent research has developed a variety of cosmological models of the Universe that explain the accelerating expansion. The notion of dark energy (DE) has recently gained prominence. DE is an exotic energy constituent with high negative pressure that explains numerous data and addresses several significant issues in modern cosmology. The second alternative is to suppose that GRT fails at large scales and that gravity may be explained via a more general action than the Einstein–Hilbert action.

In general, modified theories of gravity can be divided between models following the GRT structure with null torsion and non-metricity (such as the $f(R)$ and $f(R, T)$ theories [9–12]), models with torsion T (the teleparallel equivalent of GRT) [13,14], and models with non-metricity Q (the symmetric teleparallel equivalent of GRT) [15,16]. Here, we will examine the $f(Q)$ theory, an extension of the symmetric teleparallel equivalent GRT in which gravity is due to the non-metricity scalar Q. In $f(Q)$ theory, the covariant divergence of the metric tensor $g_{\mu\nu}$ is non-zero, and this feature can be represented mathematically in terms of a new geometric variable known as non-metricity i.e. $Q_{\gamma\mu\nu} = \nabla_\gamma g_{\mu\nu}$, which geometrically represents the variation of the length of a vector in a parallel transport process.

Recently, several intriguing cosmological and astrophysical consequences of $f(Q)$ gravity have been published, such as: The first cosmological solutions [16,17]; Quantum cosmology [18]; The coupling matter in $f(Q)$ gravity [19]; Black hole solutions [20];

* Corresponding author.
E-mail addresses: a.b.mussatayeva@gmail.com (A. Mussatayeva), nmyrzakulov@gmail.com (N. Myrzakulov), pr.mouhssine@gmail.com (M. Koussour).

https://doi.org/10.1016/j.dark.2023.101276
2212-6864/

General covariant symmetric teleparallel gravity [21]; Evidence that non-metricity of $f(Q)$ gravity can challenge ΛCDM [22]; Gravitational waves [23–25]; The acceleration of the Universe and DE [26–30]; Observational constraints [31–33].

Motivated by the previous discussion and studies on modified $f(Q)$ theory of gravity, in the present study, the accelerated expansion has been investigated using one specific parametrization of the total or effective equation of state (EoS) parameter ω_{eff} in the background of $f(Q)$ theory of gravity (Section 3 explored the fundamental features of the specified ω_{eff}). We have also considered the power-law form of $f(Q) = \beta Q^{(m+1)}$, where β and m are arbitrary constants [19]. The primary purpose of this research is to examine the nature of late-time cosmology's evolution. The observational constraints on model parameters are established by employing the Observational Hubble parameter data (*OHD*), *BAO* data, and *SNe* data. We then examined the evolution of the density parameter, the effective EoS parameter, and the deceleration parameter at the $1-\sigma$ and $2-\sigma$ confidence levels (CL) using the estimated values of model parameters. This work is structured as follows: in Section 2, we present a brief review of the $f(Q)$ gravity. In Section 3, we write the cosmological solution of the Hubble parameter by using a specific parametrization of the effective EoS parameter and a power-law model of $f(Q)$ theory. In Section 4, we calculate the values of the model parameters using the combined *OHD*+*BAO*+*SNe* data. Moreover, we describe the behavior of several parameters such as the density, EoS, and deceleration parameters. In Section 5, we examine the $Om(z)$ diagnostic parameter history of our $f(Q)$ model to see if the assumed model recognizes the DE behavior, and then we do a linear perturbation analysis. Finally, in Section 6, we summarize our findings.

2. A brief review of $f(Q)$ gravity

In general, in the presence of matter components, the action for a $f(Q)$ gravity model is written as [15,16],

$$S = \int \sqrt{-g} d^4x \left[\frac{f(Q)}{2\kappa^2} + L_m\right], \tag{1}$$

where g is the determinant of the metric tensor $g^{\mu\nu}$, i.e. $g = det(g_{\mu\nu})$, $\kappa^2 = 8\pi G = 1/M_p^2$, G is the Newtonian constant, while M_p is the reduced Planck mass. L_m denotes the Lagrangian density of the matter components. For the time being, the term $f(Q)$ is an arbitrary function of the non-metricity scalar Q.

The tensor of non-metricity and its traces are given by

$$Q_{\gamma\mu\nu} = \nabla_\gamma g_{\mu\nu}, \tag{2}$$

$$Q_\beta = g^{\mu\nu} Q_{\beta\mu\nu} \qquad \widetilde{Q}_\beta = g^{\mu\nu} Q_{\mu\beta\nu}. \tag{3}$$

Furthermore, as a function of the non-metricity tensor, the superpotential (or the non-metricity conjugate) can be expressed as,

$$P^\beta{}_{\mu\nu} = -\frac{1}{2} L^\beta{}_{\mu\nu} + \frac{1}{4}(Q^\beta - \widetilde{Q}^\beta) g_{\mu\nu} - \frac{1}{4}\delta^\beta_{(\mu} Q_{\nu)}. \tag{4}$$

where $L^\beta{}_{\mu\nu}$ is the disformation tensor,

$$L^\beta{}_{\mu\nu} \equiv \frac{1}{2} g^{\beta\sigma}\left(Q_{\nu\mu\sigma} + Q_{\mu\nu\sigma} - Q_{\beta\mu\nu}\right). \tag{5}$$

Hence, the non-metricity scalar is expressed as,

$$Q = -Q_{\beta\mu\nu} P^{\beta\mu\nu}. \tag{6}$$

Using the variation of action in Eq. (1) with respect to the metric tensor $g^{\mu\nu}$, one can obtain the field equations,

$$\frac{2}{\sqrt{-g}} \nabla_\beta \left(f_Q \sqrt{-g}\, P^\beta{}_{\mu\nu}\right) + \frac{1}{2} f\, g_{\mu\nu} + f_Q \left(P_{\mu\beta\lambda} Q_\nu{}^{\beta\lambda} - 2 Q_{\beta\lambda\mu} P^{\beta\lambda}{}_\nu\right) = -T_{\mu\nu}, \tag{7}$$

where $f_Q = \frac{df}{dQ}$. Moreover, $T_{\mu\nu}$ is the energy–momentum tensor of the cosmic fluid, which is considered to be a perfect fluid, i.e. $T_{\mu\nu} = (\rho + p) u_\mu u_\nu + p g_{\mu\nu}$, where $u^\mu = (1, 0, 0, 0)$ represents the 4-velocity vector components that form the fluid. ρ and p represent the total energy density and total pressure of any perfect fluid of matter and DE, respectively.

In the context of a flat FLRW space–time, the modified Friedmann equations

$$ds^2 = -dt^2 + a^2(t)[dx^2 + dy^2 + dz^2], \tag{8}$$

where $a(t)$ is the scale factor of the Universe are given by [19]

$$3H^2 = \frac{1}{2f_Q}\left(-\rho + \frac{f}{2}\right), \tag{9}$$

$$\dot{H} + 3H^2 + \frac{\dot{f}_Q}{f_Q} H = \frac{1}{2f_Q}\left(p + \frac{f}{2}\right), \tag{10}$$

where $Q = 6H^2$, and H denotes the Hubble parameter, which estimates the rate of expansion of the Universe. It is interesting to note that the standard Friedmann equations of GR can be found if the function $f(Q) = -Q$ is considered, i.e. $3H^2 = \rho$ and $2\dot{H} + 3H^2 = -p$.

In our study, we consider a simplified cosmological scenario where the universe is composed of two main components: matter and DE. The matter is assumed to be fluid without pressure ($p_m = 0$), while DE is considered to possess negative pressure, which is responsible for driving the observed cosmic acceleration. For this reason, we assume that $\rho = \rho_m + \rho_{DE}$ and $p = p_{DE}$. In addition, the equation of state (EoS) parameter is a quantity used in cosmology to explain the properties of DE. The effective or total EoS parameter is defined as the ratio of the total pressure to the total energy density. In the context of our study, it takes into account contributions from various cosmic components, including DE and matter. Therefore, the effective EoS parameter, denoted as ω_{eff}, is given by

$$\omega_{eff} = \frac{p}{\rho} = -1 + \frac{\left(\dot{H} + \frac{\dot{f}_Q}{f_Q} H\right)(2f_Q)}{\left(\frac{f}{2} - 6H^2 f_Q\right)}. \tag{11}$$

The above dot symbolizes the differentiation with regard to cosmic time t. Furthermore, the EoS parameter which combines the energy density and pressure of the DE component is,

$$\omega_{DE} = \frac{p_{DE}}{\rho_{DE}} \tag{12}$$

Now, in order to derive the matter conservation equation, we can be taking the trace of the field equation,

$$\dot{\rho}_m + 3\rho_m H = 0, \tag{13}$$

By solving Eq. (13), we are able to derive the solution for the energy density of the matter ρ_m as,

$$\rho_m = \rho_{m0} a^{-3}, \tag{14}$$

where ρ_{m0} is the present value of the energy density of the matter.

3. Late-time cosmological evolution via a specific type of EoS parameter

This section examines the Universe's evolution at late times using a specific type of EoS parameter. However, the equations obtained from this analysis are complex and require numerical solutions. To simplify the implementation of such solutions, a

change of variable is performed, where the red-shift, z, is used as the dynamical variable instead of the cosmic time t. One starting point that we can rely on is that $z = \frac{a_0}{a(t)} - 1$, where a_0 is the present time of the scale factor. For simplicity, the scale factor is set to 1 currently. It is not directly observable, but we can observe the ratio of the scale factor at different times to its value at the present time. The following relationship may therefore be deduced: $\frac{d}{dt} = -H(z)(1+z)\frac{d}{dz}$. Thus, it is clear that.

$$\dot{H} = -H(z)(1+z)H'(z), \tag{15}$$

where, the symbol 'prime' represents differentiation with respect to the red-shift variable, denoted by 'z'.

In this context, it is evident that we can utilize only Eqs. (9) and (10) for our analysis. However, rather than solving the ensuing equation for $H(z)$, we can introduce an effective form of the EoS parameter, which is defined as follows: $\omega_{eff} = -1 + \frac{A}{A+B(1+z)^{-3}}$, where A and B are arbitrary constants. The reason behind selecting this particular parametrization for ω_{eff} is that at high red-shift values $z \gg 1$ (early stages of cosmological evolution), ω_{eff} is nearly zero, indicating the behavior of the EoS parameter for a pressureless fluid, such as ordinary matter. As we move towards the present epoch ($z = 0$), ω_{eff} decreases gradually to negative values, leading to negative pressure and an effective EoS value $\omega_{eff} = -\frac{B}{A+B}$. In this case, the functional form of ω_{eff} is dependent on the specific values of A and B. As a result, the form of ω_{eff} can effortlessly incorporate the phases of cosmic evolution, including the early matter-dominated era and the late-time DE-dominated era. The specific form mentioned, introduced in Ref. [34], exhibits phantom-like behavior in the present epoch. Due to the presence of a large number of free parameters in the effective EoS parameter, we adopt a specific approach for the observational analysis. In order to constrain the model and facilitate the analysis, we fix the value of n to be 3. In literature, various parametrization models of EoS for DE have been proposed and fitted to observational data. Ref. [35] proposed an one-parameter family of EoS DE model. Two-parameters family of EoS DE parametrizations, especially the Chevallier–Polarski–Linder parametrization [36,37], the Linear parametrization [37–40], the Logarithmic parametrization [41], the Jassal–Bagla–Padmanabhan parametrization [42], and the Barboza–Alcaniz parametrization [43], were also explored. Further, in [44–46] three and four parameters family of EoS DE parametrizations are examined.

In this section, we will look at a specific cosmological model in $f(Q)$ gravity theory. We also look at how geometrical and physical cosmological parameters such as energy density, pressure, and deceleration behave under $f(Q)$ gravity. In this study, we investigate the scenario where the function $f(Q)$ can be expressed as, $f(Q) = \beta Q^{(m+1)}$, where β and m are arbitrary constants [19,47,48]. For the function $f(Q)$ we obtain the expression $f_Q = \beta(1+m)Q^m$ and $f_{QQ} = \beta(1+m)mQ^{m-1}$. By putting the above expressions for f, f_Q, and f_{QQ} into Eqs. (9) and (10) we can derive the energy density and pressure as,

$$\rho = \beta\left(-2^m\right)3^{m+1}(2m+1)H^{2(m+1)}, \tag{16}$$

and

$$p = \beta 6^m(2m+1)H^{2m}\left(2\dot{H}(m+1)+3H^2\right). \tag{17}$$

Now by using Eq. (11), we obtain the EoS parameter in terms of Hubble parameter and its derivative as,

$$\omega_{eff} = -1 + \frac{2(m+1)}{3}\frac{(1+z)H'(z)}{H(z)}. \tag{18}$$

By using Eq. (18) and the presumed ansatz of ω_{eff}, the evolution equation of the Hubble function takes the form

$$\frac{dH(z)}{dz} = \frac{3A(1+z)^2}{2(m+1)\left(A(1+z)^3+B\right)}H(z), \tag{19}$$

which yields the following solution

$$H(z) = H_0\left[\frac{A(z+1)^3+B}{A+B}\right]^{\frac{1}{2m+2}}, \tag{20}$$

where H_0 describes the present value (i.e. at $z = 0$) of the Hubble parameter. In particular, for the scenario $m = 0$ with $\beta = -1$, the solution reduces to $f(Q) = -Q$. In other words, it is directly related to the ΛCDM model. As a result, the equation for Hubble parameter $H(z)$ is reduced to $H(z) = H_0\left[\Omega_m^0(1+z)^3+\Omega_\Lambda^0\right]^{\frac{1}{2}}$, where $\Omega_m^0 = \frac{A}{A+B}$ and $\Omega_\Lambda^0 = \left(1-\Omega_m^0\right) = \frac{B}{A+B}$ are the present density parameters for matter and the cosmological constant, respectively. As a result, the model parameter m is an excellent indicator of the present model's deviation from the ΛCDM model due to the addition of non-metricity terms.

The deceleration parameter q is one of the cosmological parameters that is important in describing the status of our Universe's expansion. If the value of the deceleration parameter is strictly less than zero, the cosmos accelerates; when it is non-negative, the cosmos decelerates. The deceleration parameter q is defined as $q(z) = -\frac{\ddot{a}}{aH^2} = -1 + \frac{(1+z)}{H(z)}\frac{dH(z)}{dz}$. In this scenario, the expression of the deceleration parameter is

$$q(z) = -1 + \frac{3A(1+z)^3}{2(m+1)\left(A(1+z)^3+B\right)}. \tag{21}$$

The behavior and important cosmological features of the model represented in Eq. (20) are entirely reliant on the model parameters (A, B, and m). In the next part, we use current observational data to study the behavior of the cosmological parameters to constrain the model parameters (A, B, and m).

4. Method of data fitting

In our research, we took into account the most current and relevant observational findings:

- **Observational Hubble parameter Data** (*OHD*): We examine $H(z)$ data points calculated by employing differential galaxy ages as a function of red-shift z and line-of-sight *BAO* data. [49–51].
- **Baryon Acoustic Oscillation** (*BAO*): We additionally take into account the *BAO* data from the SDSS-MGS, Wiggle Z, and 6dFGS projects [52–54].
- **Type-Ia Supernova measurement** (*SNe* Ia): We examine the Pantheon sample of 1048 SNe Ia luminosity distance values from the Pan-STARSS1 (PS1) Medium Deep Survey, the Low-z, SDSS, SNLS, and HST missions [55,56].

In addition, for likelihood minimization, we employ the MCMC (Markov Chain Monte Carlo) sample from the Python package *emcee* [57] , which is commonly used in astrophysics and cosmology to investigate the parameter space $\theta_s = (A, B, m)$. To do this, we are now focusing on three data: *OHD*, *BAO*, and *SNe* Ia data. We evaluate the priors on the parameters $-10.0 < A < 10.0$, $-10.0 < B < 10.0$, and $-10.0 < m < 10.0$. To find out the outcomes of our MCMC study, we employed 100 walkers and 1000 steps. The discussion about the observational data has also been presented in a very similar fashion in Ref. [2], shedding further light on the significance of these findings. In the following subsections of our manuscript, we provide further detailed discussions on the observational data used, as well as the statistical analyses employed. We aim to present a comprehensive and transparent description of our methodology, emphasizing the novelty and contributions of our work while acknowledging the commonalities with existing literature.

4.1. OHD

We utilize a commonly popular compilation with an updated set of 57 data points. In this collection of 57 Hubble data points, 31 were measured using the method of differential age (DA), while the remaining 26 were measured using *BAO* and other methods in the red-shift range provided as $0.07 \leq z \leq 2.42$, allowing us to determine the expansion rate of the Universe at red-shift z. Hence, the Hubble parameter $H(z)$ as a function of red-shift can be written as

$$H(z) = -\frac{1}{1+z}\frac{dz}{dt}. \tag{22}$$

To calculate the mean values of the model parameters A, B, and m, we used the chi-square function (χ^2) for *OHD* as,

$$\chi^2_{OHD} = \sum_{i=1}^{57} \frac{[H(\theta_s, z_i) - H_{obs}(z_i)]^2}{\sigma(z_i)^2}, \tag{23}$$

where $H(z_i)$ denotes the theoretical value for a specific model at different red-shifts z_i, and $H_{obs}(z_i)$ denotes the observational value, $\sigma(z_i)$ denotes the observational error.

4.2. BAO

We employ a compilation of SDSS, 6dFGS, and Wiggle Z surveys at various red-shifts for *BAO* data. This paper incorporates *BAO* data as well as the cosmology listed below,

$$d_A(z) = c\int_0^z \frac{dy}{H(y)}, \tag{24}$$

$$D_v(z) = \left[\frac{d_A^2(z)cz}{H(z)}\right]^{1/3}, \tag{25}$$

where $d_A(z)$ represents the comoving angular diameter distance, and D_v represents the dilation scale. Moreover, the chi-square function (χ^2) for *BAO* is given by

$$\chi^2_{BAO} = X^T C^{-1}_{BAO} X. \tag{26}$$

Here, X depends on the considered survey and C^{-1}_{BAO} represents the inverse covariance matrix [54].

4.3. SNe

To obtain the best values using SNe Ia, we begin with the measured distance modulus μ_{obs} produced from SNe Ia detections and compare it to the theoretical value μ_{th}. The Pantheon sample, a recent SNe Ia dataset containing 1048 points of distance modulus μ_{obs} at various red-shifts in the range $0.01 < z < 2.26$, is taken into consideration in this work. The distance modulus of each SNe can be calculated using the following equations:

$$\mu_{th}(z) = 5log_{10}\frac{d_l(z)}{Mpc} + 25, \tag{27}$$

$$d_l(z) = c(1+z)\int_0^z \frac{dy}{H(y,\theta)}. \tag{28}$$

where c is the speed of light. The distance modulus can be calculated using the relationship,

$$\mu = m_B - M_B + \alpha x_1 - \beta\, c + \Delta_M + \Delta_B, \tag{29}$$

where m_B is the measured peak magnitude at the B-band maximum, and M_B is the absolute magnitude. The parameters c, α, β, and x_1, respectively, correspond to the color at the brightness point, the luminosity stretch-color relation, and the light color shape. Moreover, Δ_M and Δ_B are distance adjustments based on the host galaxy's mass and simulation-based anticipated biases. The nuisance parameters in the above equation were obtained using a novel method known as BEAMS with Bias Corrections (BBC) [58]. As a result, the measured distance modulus is equal to the difference between the apparent magnitude m_B and the absolute magnitude M_B i.e., $\mu = m_B - M_B$. For the Pantheon data, the χ^2 function is assumed to be,

$$\chi^2_{SNe} = \sum_{i,j=1}^{1048} \Delta\mu_i \left(C^{-1}_{SNe}\right)_{ij} \Delta\mu_j \tag{30}$$

where $\Delta\mu_i = \mu_{th} - \mu_{obs}$ and C_{SNe} represents the covariance matrix.

4.4. OHD + BAO + SNe

Now, the χ^2 function for the *OHD*+*BAO*+*SNe* data is assumed to be,

$$\chi^2_{total} = \chi^2_{OHD} + \chi^2_{BAO} + \chi^2_{SNe}, \tag{31}$$

By using the aforementioned combined *OHD*+*BAO*+*SNe* data, we obtained the best-fit values of the model parameters A, B, and m, as shown in Fig. 1 with $1-\sigma$ and $2-\sigma$ likelihood contours. The best-fit values obtained are $A = 0.342^{+0.022}_{-0.022}$, $B = 0.677^{+0.025}_{-0.025}$, and $m = 0.013^{+0.021}_{-0.021}$. For $m = 0$, Fig. 2 shows the results of $1-\sigma$ and $2-\sigma$ likelihood contours with the best-fit values of model parameters are $A = 0.3353 \pm 0.0010$, and $B = 0.6837 \pm 0.0019$. Figs. 3 and 4

also show the error bars for $H(z)$ and $\mu(z)$ using $H_0 = (67.4 \pm 0.5)\ Km/s/Mpc$ [59]. The figures also show a comparison of our model to the commonly used ΛCDM model in cosmology i.e. $H(z) = H_0\sqrt{\Omega^0_m (1+z)^3 + \Omega^0_\Lambda}$ (we have considered $\Omega^0_m = 0.315 \pm 0.007$) [59]. As shown in the figures, our model matches the observed data nicely.

We will now discuss the cosmological consequences of the obtained observational constraints. Using the obtained mean values of the model parameters A, B, and m constrained by the combined *OHD*+*BAO*+*SNe* data, we investigate the behavior of the density, the EoS, and the deceleration parameters.

In Figs. 5, 6, and 7, we presented the density parameter, EoS parameter, and deceleration parameter as a function of red-shift for the combined *OHD* + *BAO* + *SNe* data. From Fig. 5, it can be observed that as the universe expands, both the matter density parameter and the DE density parameter exhibit a decrease. In the late stages, the matter density approaches zero, while the DE density converges towards a small value. In addition, the densities parameter behaves positively for model parameter values constrained by the combined *OHD* + *BAO* + *SNe* data.

As mentioned in Section 2, the EoS parameter is a vital cosmological parameter for understanding the nature of the Universe and its history through time, and it is defined as $\omega = \frac{p}{\rho}$, where p is the pressure and ρ is the energy density. The value of the EoS parameter governs how the fluid behaves and how it affects the expansion of the Universe. For example, if $\omega = 0$, the fluid is referred to as non-relativistic matter and behaves like dust. However, if $\omega = 1/3$, the fluid is referred to as relativistic matter and behaves like radiation. If $\omega < -1/3$, the fluid is considered to have negative pressure and is responsible for the Universe's accelerated expansion, a phenomenon associated with DE, which includes the quintessence ($-1 < \omega < -1/3$) era, cosmological constant ($\omega = -1$), and phantom era ($\omega < -1$). The existing observational constraints imply that the EoS parameter of the Universe's dominating component (DE), is extremely near to -1. In other terms, the pressure of DE is negative and nearly constant, fueling the Universe's accelerated expansion. Recent investigations of the *CMB* radiation, the *LSS* of the Universe, the

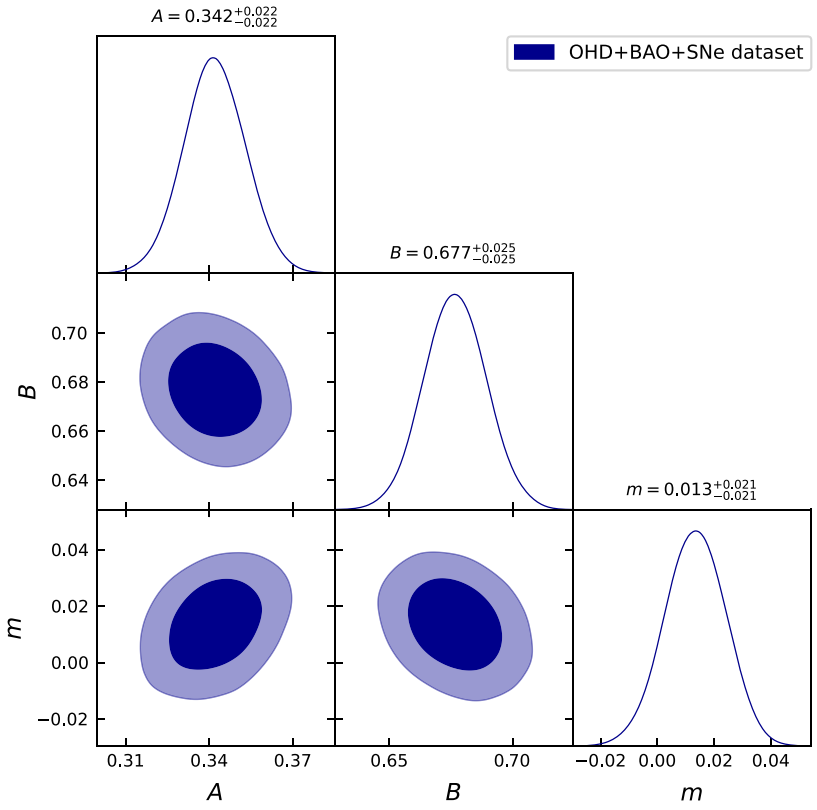

Fig. 1. The $1-\sigma$ and $2-\sigma$ confidence curves for the model parameters A, B, and m with combined $OHD + BAO + SNe$ data.

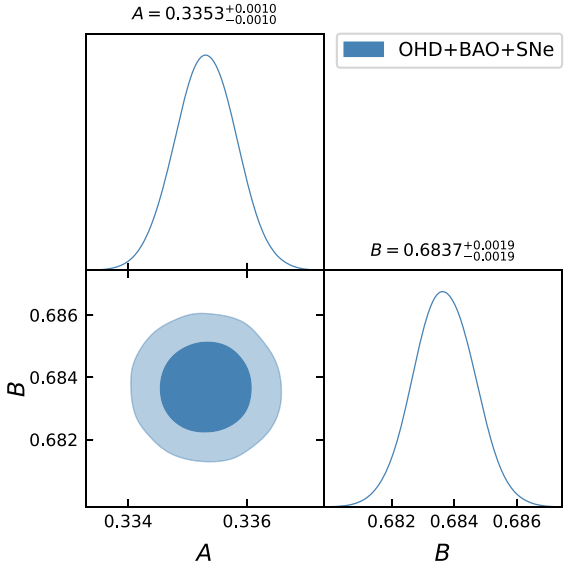

Fig. 2. The $1-\sigma$ and $2-\sigma$ confidence curves for the model parameters A, and B with combined $OHD + BAO + SNe$ data for $m = 0$.

luminosity-distance relation of *SNe* Ia, and others, have given compelling evidence for the existence of DE and its dominating role in the Universe's expansion. The most recent measurements of the EoS parameter from these data produce a value of $\omega_0 = -1.03 \pm 0.03$ [59], which is compatible with the cosmological constant.

In this paper, we focus on the analysis of an effective EoS parameter using three model parameters: A, B, and m. The behavior of the EoS parameter is depicted in Fig. 6 for constrained values of A, B, and m from the combined $OHD + BAO + SNe$ data. From the analysis conducted, it is apparent that both the evolving EoS parameter for the DE and the effective EoS parameter demonstrate quintessence-like behavior. This observation highlights the resemblance to the typical characteristics associated with quintessence, shedding light on the intriguing nature of the DE component under investigation. The present value (i.e. at $z = 0$) of the EoS parameter for DE is $\omega_0 = -0.91 \pm 0.08$ [60,61], indicating an accelerating phase.

In addition, as shown in Fig. 7, we analyzed the behavior of the deceleration parameter for constrained values of A, B, and m from the combined $OHD + BAO + SNe$ data. The sign of the deceleration parameter (q) indicates whether the model is accelerating or decelerating. If $q > 0$, the model decelerates, if $q = 0$, it expands at a steady rate, and if $-1 < q < 0$, it expands at an accelerating rate. With $q = -1$, the Universe shows exponential growth or De-Sitter expansion and super-exponential expansion for $q < -1$. In Eq. (21), we have obtained the deceleration parameter for our model. According to Fig. 7, the model transitions from a decelerated stage to an accelerated stage. It can also be seen that our model initially decelerates ($q > 0$) and then approaches exponential expansion in late times ($q = -1$). In the figure, we also compare our model to the commonly accepted ΛCDM model in cosmology. According to the constrained values of model parameters A, B, and m from the combined $OHD + BAO + SNe$ data, the present value of the transition red-shift is $z_{tr} = 0.60 \pm 0.02$ [62–64], while the present value of the deceleration parameter is $q_0 = -0.50 \pm 0.01$ [65–67], indicating that the phase is accelerating.

5. *Om*(z) diagnostic and linear perturbations

5.1. *Om*(z) Diagnostic

Sahni et al. [68] introduced the $Om(z)$ diagnostic parameter as an alternative to the statefinder parameter, which aids in

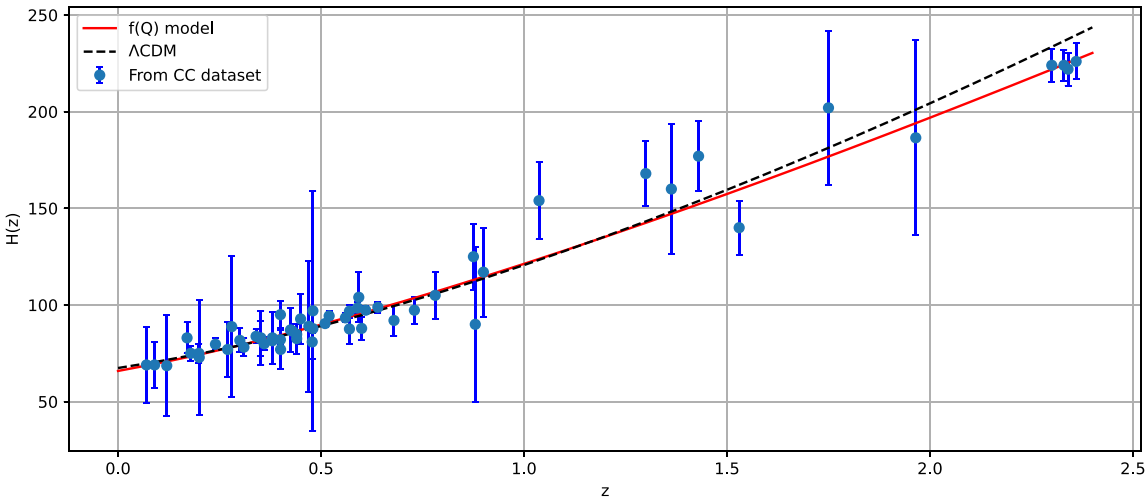

Fig. 3. The evolution of Hubble parameter $H(z)$ with regard to red-shift z. The black dashed line represents the ΛCDM model, the red line is our model's curve, and the blue dots show error bars. (For interpretation of the references to color in this figure legend, the reader is referred to the web version of this article.)

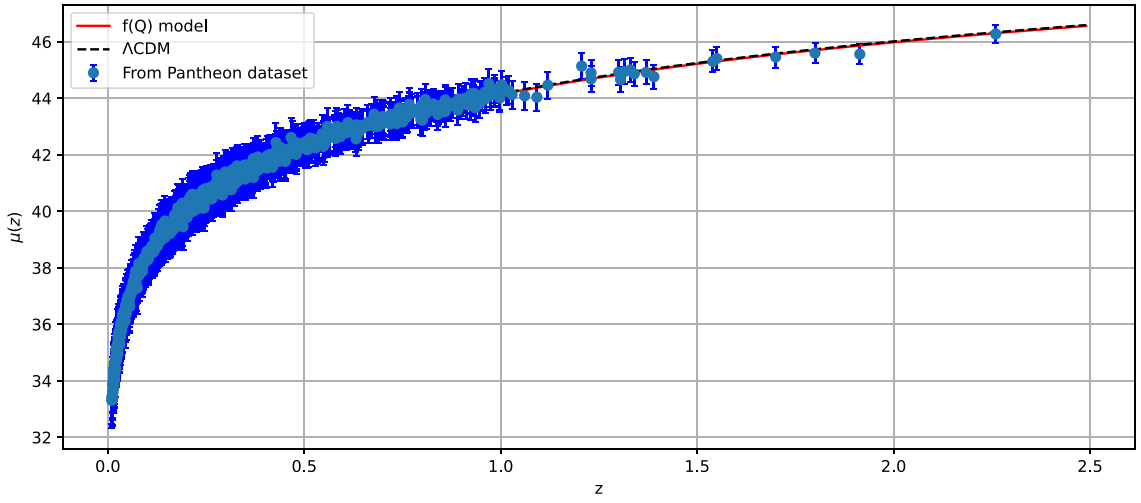

Fig. 4. The evolution of distance modulus $\mu(z)$ with regard to red-shift z. The black dashed line represents the ΛCDM model, the red line is our model's curve, and the blue dots show error bars. (For interpretation of the references to color in this figure legend, the reader is referred to the web version of this article.)

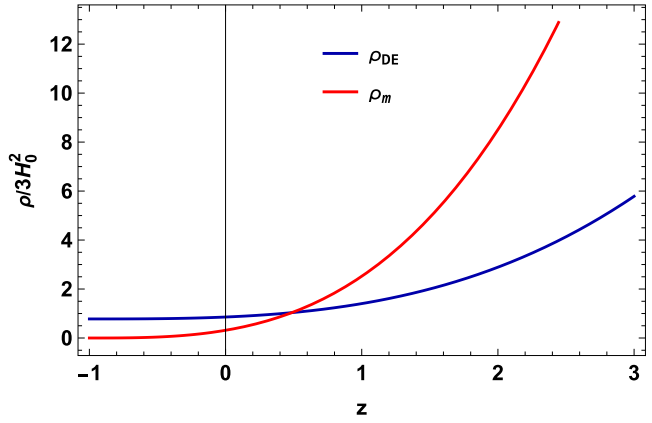

Fig. 5. Evolution of the density parameter for matter and DE from the study of the combined $OHD + BAO + SNe$ data for the best fitting values of A, B, and m.

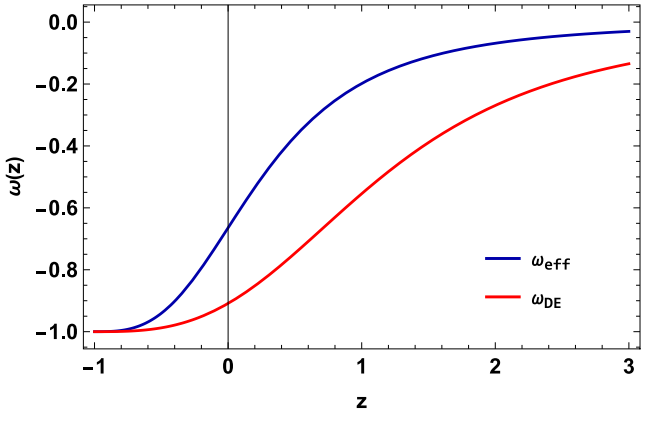

Fig. 6. Evolution of the EoS parameter from the study of the combined $OHD + BAO + SNe$ data for the best fitting values of A, and B.

distinguishing the current matter density contrast Om in various models more successfully. This is also a geometrical diagnostic that is clearly dependent on red-shift (z) and the Hubble parameter (H). It is defined as follows:

$$Om\,(z) = \frac{\left(\frac{H(z)}{H_0}\right)^2 - 1}{(1+z)^3 - 1}. \tag{32}$$

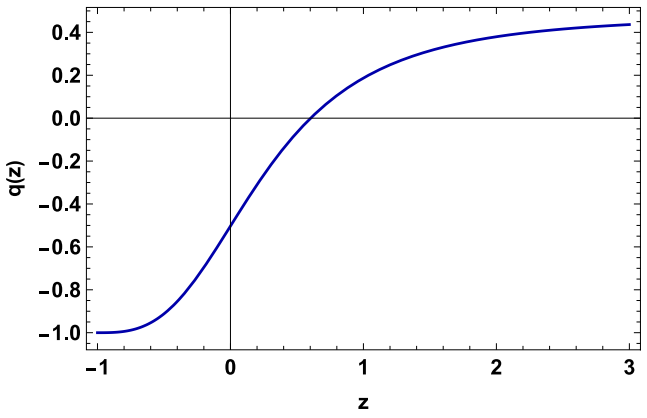

Fig. 7. Evolution of the deceleration parameter from the study of the combined $OHD + BAO + SNe$ data for the best fitting values of A, B, and m.

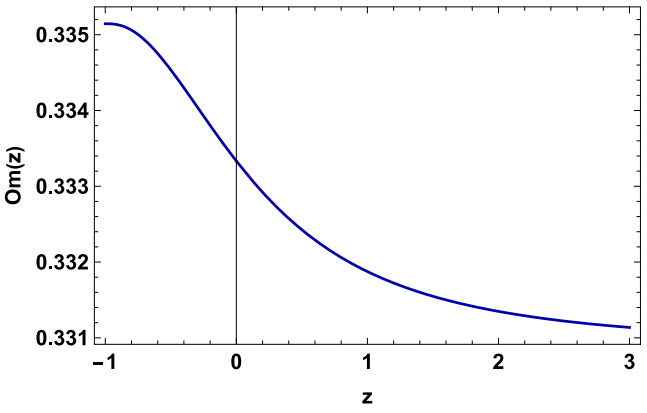

Fig. 8. Evolution of the $Om(z)$ diagnostic parameter from the study of the combined $OHD + BAO + SNe$ data for the best fitting values of A, B, and m.

The negative slope of $Om(z)$ corresponds to quintessence type behavior ($-1 < \omega < -1/3$), while the positive slope corresponds to phantom-type behavior ($\omega < -1$). The ΛCDM model ($\omega = -1$) is represented by the constant nature of $Om(z)$. According to Fig. 8, the $Om(z)$ diagnostic parameter has a negative slope throughout its entire domain. As a result of the $Om(z)$ diagnostic test, our $f(Q)$ model follows the quintessence scenario. Based on the findings, we can draw a conclusive inference that the behavior of the $Om(z)$ diagnostic parameter aligns with the behavior exhibited by the EoS parameter. The correspondence between these two parameters indicates a strong relationship, suggesting that variations in the EoS parameter are effectively captured by the $Om(z)$ diagnostic parameter. This observation underscores the utility and reliability of the $Om(z)$ parameter as a diagnostic tool for understanding the dynamics of the DE component.

5.2. Linear perturbations

In this subsection, our focus is on examining the stability of the $f(Q)$ cosmological model by analyzing the effects of linear homogeneity and isotropic perturbation. By considering small deviations from the Hubble parameter given by Eq. (20) and the energy density evolution i.e. Eq. (9), we aim to understand the behavior and robustness of the cosmological models under study. Linear perturbation analysis has been extensively used in cosmology to study the growth of structures and the evolution of the universe. Many previous studies have successfully employed linear approximations to explore the behavior of modified gravity theories and assess their compatibility with observational data [69–72]. The perturbations under consideration in this analysis are of first order,

$$\widehat{H}(t) = H(t)(1 + \delta\,(t)) \tag{33}$$

$$\widehat{\rho}(t) = \rho(t)(1 + \delta_m\,(t)), \tag{34}$$

where $\delta\,(t)$ represents the isotropic deviation of the background Hubble parameter, while $\delta_m\,(t)$ corresponds to the matter overdensity. Hence, the perturbation of the functions $f(Q)$ and f_Q can be expressed as $\delta f = f_Q \delta Q$ and $\delta f_Q = f_{QQ}\delta Q$, where $\delta Q = 12H\delta H$ is the first-order perturbation of the scalar Q. So, neglecting the higher power of $\delta\,(t)$, the Hubble parameter can be expressed as $6\widehat{H}^2 = 6H^2\,(1 + \delta\,(t))^2 = 6H^2\,(1 + 2\delta\,(t))$. Now, using Eq. (9) we get

$$Q\left(f_Q + 2Qf_{QQ}\right)\delta = -\rho\delta_m. \tag{35}$$

This gives rise to the matter-geometric perturbation relation, and the perturbed Hubble parameter can be calculated using Eq. (33). Then, just use perturbation continuity equation to get the analytical solution to the perturbation function,

$$\dot{\delta_m} + 3H(1 + \omega)\delta = 0. \tag{36}$$

Solving the above equations for δ and δ_m yields the first order differential equation,

$$\dot{\delta_m} - \frac{3H(1 + \omega)\rho}{Q(f_Q + 2Qf_{QQ})}\delta_m = 0. \tag{37}$$

Using Eqs. (9) and (10) to simplify the previous equation once more, the solution is expressed as,

$$\delta_m\,(z) = \delta_{m_0} H\,(z)\,, \tag{38}$$

and

$$\delta\,(z) = -\frac{\delta_{m0}}{3\left(1 + \omega_{eff}\right)}\frac{\dot{H}}{H}. \tag{39}$$

By using Eqs. (20) and (38), we obtain

$$\delta_m\,(z) = \delta_{m0}H_0\left(\frac{A(z+1)^3 + B}{A + B}\right)^{\frac{1}{2m+2}}. \tag{40}$$

Again, by using Eqs. (18) and (39), we obtain

$$\delta\,(z) = \frac{\delta_{m0}H_0\left(\frac{A(z+1)^3+B}{A+B}\right)^{\frac{1}{2m+2}}}{2(m+1)}. \tag{41}$$

Figs. 9 and 10 show the history of the perturbation terms $\delta_m\,(z)$ and $\delta\,(z)$ in terms of red-shift z. Both the perturbations $\delta_m\,(z)$ and $\delta\,(z)$ diminish rapidly and reach zero at late times. It may also be demonstrated that the behavior of $\delta_m\,(z)$ and $\delta\,(z)$ is the same for all model parameter values. Consequently, using the scalar perturbation approach, our $f(Q)$ model demonstrates stable behavior.

6. Conclusion

The current scenario of accelerating Universe expansion is now a significant topic of study. Two approaches have been proposed to explain this cosmic acceleration. One approach is to investigate different dynamical DE models (such as quintessence and phantom), while another is to analyze alternate gravity theories. In this paper, we investigated accelerated expansion using the FLRW Universe and the $f(Q)$ theory of gravity, particularly $f(Q) = \beta Q^{(m+1)}$, where β and m are arbitrary constants. We obtained the solution of the Hubble parameter using the

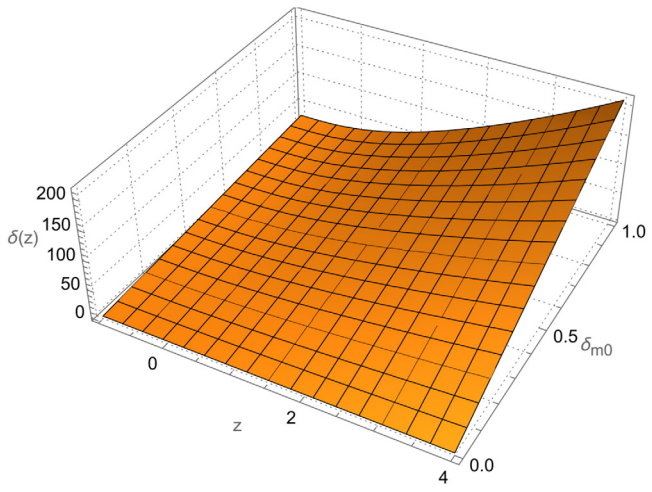

Fig. 9. Evolution of the $\delta(z)$ from the study of the combined $OHD + BAO + SNe$ data for the best fitting values of A, B, and m and different δ_{m0} values.

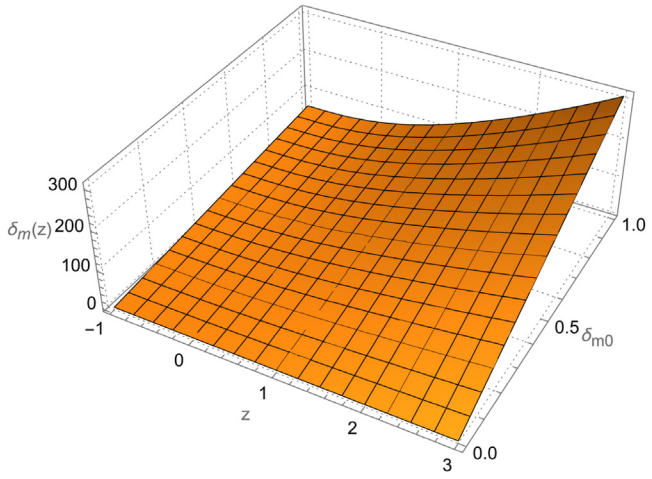

Fig. 10. Evolution of the $\delta_m(z)$ from the study of the combined $OHD+BAO+SNe$ data for the best fitting values of A, B, and m and different δ_{m0} values.

parametrization form of the effective EoS parameter as $\omega_{eff} = -1 + \frac{A}{A+B(1+z)^{-3}}$ (where A and B are arbitrary constants), which leads to a varying deceleration parameter. As shown in Section 4 of this work, we constrained model parameters (A, B, and m) using the MCMC approach with a combined analysis of *OHD*, *BAO*, and *SNe* data. The best-fit values obtained are $A = 0.342^{+0.022}_{-0.022}$, $B = 0.677^{+0.025}_{-0.025}$, and $m = 0.013^{+0.021}_{-0.021}$. For $m = 0$, the best-fit $A = 0.3353 \pm 0.0010$, and $B = 0.6837 \pm 0.0019$. Furthermore, with the constrained values of A, B, and m from the combined $OHD+BAO+SNe$ data, we analyzed the behavior of the density parameter, EoS parameter, and deceleration parameter as a function of red-shift, as shown in Figs. 5, 6, and 7. Fig. 5 shows that both the matter density parameter and the DE density parameter are increasing functions of red-shift and exhibit the expected positive behavior. The evolution of the EoS parameter in Fig. 6 supported the accelerating nature of the Universe's expansion phase, and the model behaves like a quintessence in the present. Furthermore, the present value of the EoS parameter for DE is estimated to be $\omega_0 = -0.91 \pm 0.08$. Fig. 7 indicates that the model transitions from a decelerated stage to an accelerated stage. The present value of the transition red-shift is $z_{tr} = 0.60 \pm 0.02$ based on constrained values of model parameters A, B, and m from the combined $OHD + BAO + SNe$ data, whereas the present value of the deceleration parameter is $q_0 = -0.50 \pm 0.01$, showing that the phase is accelerating.

Then we evaluated the $Om(z)$ diagnostic parameter for our presumed $f(Q)$ model. As a result, we observed that the behavior of the $Om(z)$ diagnostic parameter conforms to the behavior of the effective EoS parameter. Lastly, the perturbation terms shown in Figs. 9 and 10 confirmed that the model is stable under the scalar perturbation method. Based on our analysis, we reach a compelling conclusion that our $f(Q)$ cosmology, incorporating the effective EoS parameter form, offers a highly efficient framework for explaining various late-time cosmic phenomena in the Universe. The fact that this model demonstrates observational validity further supports its credibility and reliability.

CRediT authorship contribution statement

A. Mussatayeva: Concept, Design, Analysis, Writing, or revision of the manuscript. **N. Myrzakulov:** Concept, Design, Analysis, Writing, or revision of the manuscript. **M. Koussour:** Concept, Design, Analysis, Writing, or revision of the manuscript.

Declaration of competing interest

From the authors no conflict of interest to declare.

Data availability

No data was used for the research described in the article.

Acknowledgments

This research is funded by the Science Committee of the Ministry of Science and Higher Education of the Republic of Kazakhstan (Grant No. AP09058240).

References

[1] A.G. Riess, et al., Astron. J. 116 (1998) 1009.
[2] S. Perlmutter, et al., Astrophys. J. 517 (1999) 565.
[3] D.J. Eisenstein, et al., Astrophys. J. 633 (2005) 560.
[4] W.J. Percival, et al., Mon. Not. R. Astron. Soc. 401 (2010) 2148.
[5] R.R. Caldwell, M. Doran, Phys. Rev. D 69 (2004) 103517.
[6] Z.Y. Huang, et al., J. Cosmol. Astropart. Phys. 0605 (2006) 013.
[7] T. Koivisto, D.F. Mota, Phys. Rev. D 73 (2006) 083502.
[8] S.F. Daniel, Phys. Rev. D 77 (2008) 103513.
[9] S. Capozziello, V.F. Cardone, V. Salzano, Phys. Rev. D 78 (2008) 063504.
[10] S. Nojiri, S.D. Odintsov, Phys. Lett. B 657 (2007) 238.
[11] T. Harko, et al., Phys. Rev. D 84 (2011) 024020.
[12] D. Momeni, R. Myrzakulov, E. Gudekli, Int. J. Geom. Methods Mod. Phys. 12 (2015) 1550101.
[13] S. Capozziello, et al., Phys. Rev. D 84 (2011) 043527.
[14] R.C. Nunes, S. Pan, E.N. Saridakis, J. Cosmol. Astropart. Phys. 08 (2016) 011.
[15] J.B. Jimenez, et al., Phys. Rev. D 98 (2018) 044048.
[16] J.B. Jimenez, et al., Phys. Rev. D 101 (2020) 103507.
[17] W. Khyllep, et al., Phys. Rev. D 103 (2021) 103521.
[18] N. Dimakis, A. Paliathanasis, T. Christodoulakis, Class. Quantum Gravity 38 (2021) 22.
[19] T. Harko, et al., Phys. Rev. D 98 (2018) 084043.
[20] F.D. Ambrosio, et al., Phys. Rev. D 105 (2022) 024042.
[21] M. Hohmann, Phys. Rev. D 104 (2021) 124077.
[22] F.K. Anagnostopoulos, S. Basilakos, E. N.Saridakis, Phys. Lett. B 822 (2021) 136634.
[23] M. Hohmann, Phys. Rev. D 99 (2009) 024009.
[24] B.J. Barros, et al., Phys. Dark Universe 30 (2020) 100616.
[25] I. Soudi, et al., Phys. Lett. B 100 (2019) 044008.
[26] M. Koussour, et al., Phys. Dark Universe 36 (2022) 101051.
[27] M. Koussour, et al., J. High Energy Phys. 37 (2023) 15–24.
[28] M. Koussour, M. Bennai, Chinese J. Phys. 79 (2022) 339–347.
[29] M. Koussour, et al., Ann. Physics 445 (2022) 169092.
[30] M. Koussour, et al., J. High Energy Astrophys. 35 (2022) 43–51.
[31] R. Lazkoz, et al., Phys. Rev. D 100 (2019) 104027.
[32] I. Ayuso, R. Lazkoz, V. Salzano, Phys. Rev. D 103 (2021) 063505.
[33] S.A. Narawade, B. Mishra, (2022) arXiv preprint arXiv:2211.09701.

[34] A.A. Mamon, Internat. J. Modern Phys. D 26 (2017) 1750136.
[35] Y.g. Gong, Y.Z. Zhang, Phys. Rev. D 72 (2005) 043518.
[36] M. Chevallier, D. Polarski, Internat. J. Modern Phys. D 10 (2001) 213.
[37] E.V. Linder, Phys. Rev. Lett. 90 (2003) 091301.
[38] A.R. Cooray, D. Huterer, Astrophys. J. 513 (1999) L95.
[39] P. Astier, Phys. Lett. B 500 (2001) 8.
[40] J. Weller, A. Albrecht, Phys. Rev. D 65 (2002) 103512.
[41] G. Efstathiou, Mon. Not. R. Astron. Soc. 310 (1999) 842.
[42] H.K. Jassal, J.S. Bagla, T. Padmanabhan, Phys. Rev. D 72 (2005) 103503.
[43] E.M. Barboza Jr., J.S. Alcaniz, Phys. Lett. B 666 (2008) 415.
[44] E.V. Linder, D. Huterer, Phys. Rev. D 72 (2005) 043509.
[45] A. De Felice, S. Nesseris, S. Tsujikawa, J. Cosmol. Astropart. Phys. 1205 (2012) 029.
[46] R.J.F. Marcondes, S. Pan, (2017) arXiv preprint arXiv:1711.06157.
[47] M. Koussour, et al., Nucl. Phys. B. 990 (2023) 116158.
[48] M. Koussour, A. De, Eur. Phys. J. C 83 (2023) 400.
[49] Yu B. Ratra, F-Yin Wang, Astrophys. J. 856 (2018) 3.
[50] M. Moresco, Mon. Not. R. Astron. Soc. 450 (2015) L16–L20.
[51] G.S. Sharov, V.O. Vasilie, Math. Model. Geom. 6 (2018) 1.
[52] C. Blake, et al., Mon. Not. R. Astron. Soc. 418 (2011) 1707.
[53] W.J. Percival, et al., Mon. Not. R. Astron. Soc. 401 (2010) 2148.
[54] R. Giostri, et al., J. Cosmol. Astropart. Phys. 1203 (2012) 027.
[55] D.M. Scolnic, et al., Astrophys. J 859 (2018) 101.
[56] Z. Chang, et al., Chin. Phys. C 43 (2019) 125102.
[57] D.F. Mackey, et al., Publ. Astron. Soc. Pac. 125 (2013) 306.
[58] R. Kessler, D. Scolnic, Astrophys. J. 836 (2017) 56.
[59] Planck Collaboration, Astron. Astrophys. 641 (2020) A6.
[60] A. Hernandez-Almada, et al., Eur. Phys. J. C 79 (2019) 12.
[61] C. Gruber, O. Luongo, Phys. Rev. D 89 (2014) 103506.
[62] O. Farooq, et al., Astrophys. J. 835 (2017) 26–37.
[63] J.F. Jesus, et al., J. Cosmol. Astropart. Phys. 04 (2020) 053–070.
[64] J.R. Garza, et al., Eur. Phys. J. C 79 (2019) 890.
[65] S. Capozziello, R.D. Agostino, O. Luongo, Mon. Not. R. Astron. Soc. 494 (2020) 2576.
[66] S.A. Al Mamon, S. Das, Eur. Phys. J. C 77 (2017) 495.
[67] S. Basilakos, F. Bauera, J. Sola, J. Cosmol. Astropart. Phys. 01 (2012) 050–079.
[68] V. Sahni, A. Shafieloo, A.A. Starobinsky, Phys. Rev. D 78 (2008) 103502.
[69] G. Farrugia, J.L. Said, Phys. Rev. D 94 (2016) 124054.
[70] A. de la C-Dombriz, D. S-Gomez, Classical Quantum Gravity 29 (2012) 245014.
[71] F.K. Anagnostopoulos, S. Basilakos, E.N. Saridakis, Phys. Lett. B 822 (2021) 136634.
[72] S.A. Narawade, et al., Phys. Dark Universe 36 (2022) 101020.